

Fractal behavior of the shortest path between two lines in percolation systems

Gerald Paul,¹ Shlomo Havlin,^{1,2} and H. Eugene Stanley¹

¹Center for Polymer Studies and Department of Physics, Boston University, Boston, Massachusetts 02215

²Minerva Center and Department of Physics, Bar-Ilan University, Ramat Gan, Israel

(Received 4 March 2002; published 13 June 2002)

Using Monte Carlo simulations, we determine the scaling form for the probability distribution of the shortest path l between two lines in a three-dimensional percolation system at criticality; the two lines can have arbitrary positions, orientations, and lengths. We find that the probability distributions can exhibit up to four distinct power-law regimes (separated by crossover regimes) with exponents depending on the relative orientations of the lines. We explain this rich fractal behavior with scaling arguments.

DOI: 10.1103/PhysRevE.65.066105

PACS number(s): 64.60.Fr, 05.45.Df, 64.60.Ak

I. INTRODUCTION

There has been considerable recent activity [1–5] analyzing $P(l|r)$, the probability distribution for the length of the shortest path, l , between two points separated by Euclidean distance r in a percolation system [6–9]. This paper extends that work by determining the scaling form of the distribution of shortest paths between two lines of arbitrary position, relative orientation and lengths in three-dimensional (3D) systems. These configurations are important because they much more realistically model the configurations used in oil recovery in which fluid is injected in one well (one of the lines in our configuration) and oil is recovered at a second well (the second line in our configuration); the wells may, in reality, be at arbitrary orientation and of different lengths. An important quantity in oil exploration is the “breakthrough time” or “first passage time,” the elapsed time for the injected fluid to first reach the second well [10,11]. Because the shortest paths between the two wells is strongly correlated with the breakthrough times [3] and the shortest paths can be modeled more efficiently than the breakthrough time, we study the distributions of shortest paths here to obtain insights into the behavior of the breakthrough time distributions.

The scaling form for the two-points configuration in which the two points are located at $[(L-r)/2, L/2, L/2], [(L+r)/2, L/2, L/2]$ in a system of side L has been found to be [1]

$$P(l|r) \sim \frac{1}{r^{d_{\min}}} \left(\frac{l}{r^{d_{\min}}} \right)^{-g_l} f_1 \left(\frac{l}{r^{d_{\min}}} \right) f_2 \left(\frac{l}{L^{d_{\min}}} \right), \quad (1)$$

where

$$f_1(x) = e^{-ax^{-\phi}} \quad (2)$$

and

$$f_2(x) = e^{-bx^\psi}. \quad (3)$$

The exponents g_l , d_{\min} , ϕ , and ψ are universal and the constants a and b depend on lattice type. In 3D, the values of these exponents have previously been found to be [3] $g_l = 2.3 \pm 0.1$, $d_{\min} = 1.39 \pm 0.05$, $\phi = 2.1 \pm 0.5$, and $\psi = 2.5$

± 0.5 . The first stretched exponential function, f_1 , reflects the fact that the shortest path must always be at least equal to the distance r between the two points; the second stretched exponential function, f_2 , reflects the fact that the lengths of the shortest paths are bounded because of the finite size L of the system.

We find that the scaling form for the two-lines configuration has the same form as that found for the shortest path distribution between two points with the exceptions that (i) the power-law regime of the distribution as represented by the term $(l/r^{d_{\min}})^{-g_l}$ in Eq. (1) is replaced with up to four different power-law regimes (separated by crossover regimes) with exponents depending on the relative orientations of the lines and (ii) the Euclidean distance r in Eq. (1) between the two points is replaced by the shortest Euclidean distance between the two lines. The lengths of the lines affect the ranges of the power-law regimes.

II. SIMULATIONS

Monte Carlo simulations were performed using the Leath method and growing clusters from two sets of seeds—one for each line. The length of the shortest path between the two lines is the sum of the chemical distances from each set of seed sites to the point where a cluster started at one set of seeds meets a cluster started from the other set of seeds [4]. The cluster growth for a given realization is terminated when the two clusters meet. For parallel line configurations, in which the probability distributions decay rapidly, we use the method of Ref. [12] to obtain good statistics for shortest paths that have very low probabilities. We use the memory management technique described in Ref. [13] to perform simulations in which the growing clusters never hit a boundary of the system.

The clusters that are created and included in our analysis are of all sizes, not just the incipient infinite cluster.

III. NONPARALLEL WELLS

A. Coplanar lines

1. Equal length symmetric lines

We start by considering relatively simple configurations of the type shown in Fig. 1(a) in which the lines are coplanar,

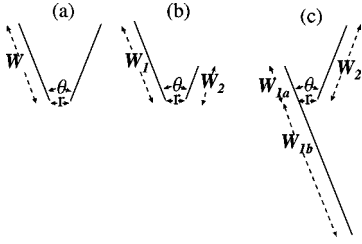


FIG. 1. Example configurations of two nonparallel lines which are studied. (a) Simple configuration of lines of equal length. (b) Configuration of lines of unequal length ($W_1 > W_2$). (c) Configuration in which the shortest distance between lines does not terminate at the ends of lines ($W_{a1} < W_2 < W_{1b}$).

of equal length, and are positioned symmetrically. We will study configurations in which the lines are of unequal length [see Fig. 1(b)] and/or are not positioned symmetrically [see Fig. 1(c)] in the following sections. In all of these configurations, r is the shortest Euclidean distance between the two lines.

Figure 2 contains log-log plots of $P(l|r)$, the shortest path distribution for $r=8$ and various values of θ . We have chosen $r=8$ so that the initial cutoff is present; for smaller values of r , lattice effects destroy this initial cutoff. Since the focus of this paper is the power-law regimes, not the initial or final cutoffs, in all later figures we will choose configurations with $r=1$ so that the power-law regime is as long as possible. The exception to this will be cases in which θ is very small where small r introduces other lattice effects.

We note that after the initial peak in each distribution, there is a power-law regime, the slope of which, $g_l(\theta)$, increases with increasing θ . We will call this power-law regime the “two-lines regime.” Simple scaling arguments imply that if the lengths of the lines were infinite, these two-line regimes would continue indefinitely. For finite line lengths, we would expect that, for large l , the distributions would exhibit a crossover to a power-law regime with the same exponent as that for a configuration with two points—because for large l the long paths travel far enough away from the lines that they appear to be points. In this regime, the power-law exponent has the value of that of two points, 2.35 [3]. For the plots in Fig. 2, in order to see the power

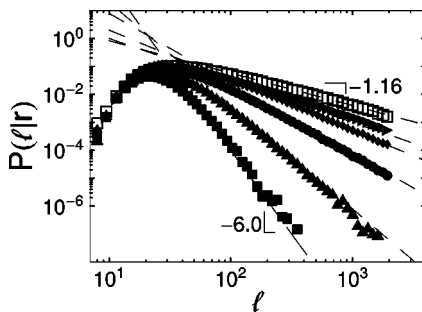


FIG. 2. $P(l|r)$ vs l for configuration of two lines of equal length with $r=8$, $\theta=$ (from bottom to top) 3° (filled square), 6° , 12° , 20° , 40° , and 180° (unfilled square). The corresponding well lengths W are 4890, 2445, 1224, 737, 374, and 128, respectively. The plots are normalized such that the initial sections of plots are coincident.

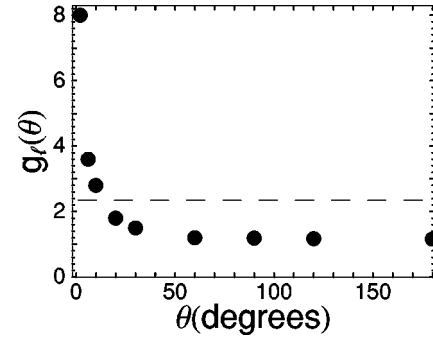


FIG. 3. The exponent of the power-law regime of $P(l|r)$, $g_l(\theta)$, for two lines vs θ . The dashed line is $g_l(\theta)=2.35$, the value of g_l for two points.

regimes clearly, we have chosen the lengths of the lines long enough that this crossover occurs after the maximum value of l in the plots.

In Fig. 3, we plot $g_l(\theta)$ vs θ . The plot suggests that $g_l(\theta)$ diverges as θ goes to zero. At θ below $\theta_c \approx 15^\circ$, $g_l(\theta)$ is greater than g_l , the power-law regime exponent for the two-points configuration. Above θ_c , $g_l(\theta)$ is less than g_l .

For two lines oriented at an angle less than θ_c , our results are consistent with the qualitative argument that the slope of the power-law regime should be greater than the slope of the power-law regime for two points because there are more ways to connect the two lines and the probability that there will be long paths is decreased. For $\theta > \theta_c$, however, where our results indicate that the slope of the power-law regime for the two-lines configuration is smaller than the slope of the power-law regime for two points, it is less clear how to explain the behavior.

The crossover between the two-line regime and the two-point regime is illustrated in Fig. 4 where in each panel we plot $P(l|r)$ for fixed θ , and various values of W . As expected, the larger the length of the lines, the higher the value of \hat{l} , the value of l at which the crossover occurs. Quantitative analysis of the crossover behavior is given in Sec. III C.

2. Point-line configurations

We next study configurations in which one line has zero length (i.e., a point) and the other is a line of finite length. This is the extreme case of the configuration in which the two lines have different lengths. We will study the case where both lines have finite lengths in the following section. We in fact study the three configurations shown in Figs. 5(a)–5(c). The plots of $P(l|r)$ for these configurations are shown in Fig. 6. The plots have a power-law regime with exponent -1.75 for the configurations of Figs. 5(a) and 5(c), and exponent -2.2 for the configuration of Fig. 5(b). We denote this regime as the “point-line regime.” Figure 7 shows the crossover from point-line behavior to two-points behavior.

3. Unequal length symmetric lines

We can now study configurations of the type shown in Fig. 1(b) in which the lines are of different lengths, W_1 and

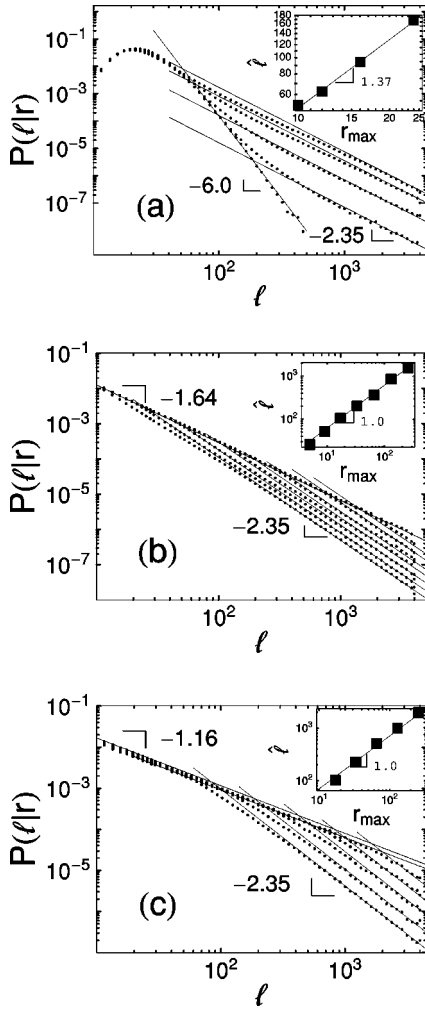


FIG. 4. $P(l|r)$ vs l for configuration of two lines of equal length. (a) $r=8$, $\theta=3^\circ$, $W=($ from top to bottom) 38, 76, 152, 304, 1216, and 2432 (b) $r=1$, $\theta=29^\circ$, $W=($ from bottom to top) 8, 17, 33, 66, 132, 265, and 529, (c) $r=1$, $\theta=180^\circ$, $W=($ from bottom to top) 8, 16, 32, 64, and 128. For all plots, the larger the value of W , the larger the value of l at which behavior changes from two-lines behavior to two-points behavior for which the slope is -2.35 . The insets plot the crossover value \hat{l} vs r_{\max} .

W_2 . For such a configuration we would expect three power-law regimes: (i) for small l such that the two lines appear to be infinite, a two-line regime, with slope dependent on θ , (ii) a point-line regime, with slope -1.75 , for values of l large enough that the shorter line appears to be a point, and (iii) a

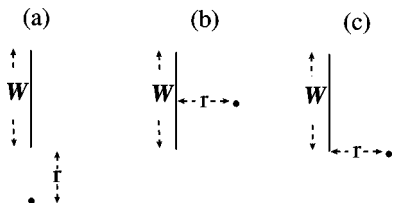


FIG. 5. Example configurations in which one line is of finite length W and one is of zero length (i.e., a point). In all cases, the shortest distance between the point and the line is r .

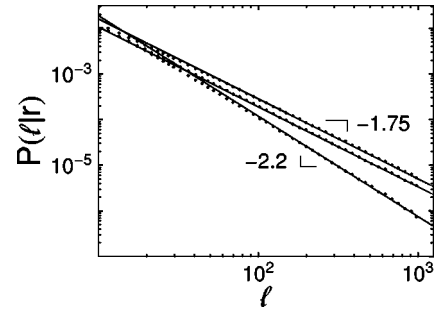


FIG. 6. $P(l|r)$ vs l for configuration of a point and a line with $r=1$ and $W=128$. From top to bottom, the plots are for the configurations shown in Figs. 5(a), 5(c), and 5(b), respectively. We see that the slopes in configurations where the point is closest to the end of the line [Figs. 5(a) and 5(c)] are the same (with some initial difference) and they are different from the slope in the configurations in which the point is closest to the middle of the line [Fig. 5(b)].

two-point regime, for even larger values of l where both lines appear to be points. Plots of $P(l|r)$ for such configurations are shown in Fig. 8 and are consistent with our expectations.

4. Complex configurations (unequal length nonsymmetric lines)

The last of the coplanar configurations is of the type shown in Fig. 1(c). In general, based on the reasoning above, for configurations of this type we would expect $P(l|r)$ to have four power-law regimes. For the configuration shown in Fig. 1(c), in which $W_{1a} \ll W_2 \ll W_{1b}$, the power-law regimes would be as follows: (i) a power-law regime corresponding to the angle θ between the segments W_{1a} and W_2 , (ii) a power-law regime corresponding to the angle $\pi - \theta$ between segments W_2 and W_{1b} , (iii) a point-line power-law regime entered when $l \geq W_{1b}$, and (iv) the two-points regime. Figure 9 is a plot of $P(l|r)$ which shows this behavior.

B. Noncoplanar lines

For noncoplanar lines, for $l \geq r$, the fact that the lines are not coplanar should be irrelevant; what is relevant is the effective angle between the lines. This angle is obtained by

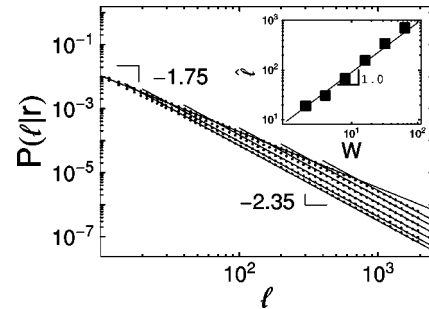


FIG. 7. $P(l|r)$ vs l for configuration of a point and a line in which the point is closest to the end of the line with $r=1$ and $W=($ from bottom to top) 2, 4, 8, 16, 32, 64, and 128. For all plots, the larger the value of W , the larger the value of $l \cong \hat{l}$ at which the behavior changes from point-line behavior to two-points behavior. The inset plots \hat{l} vs W .

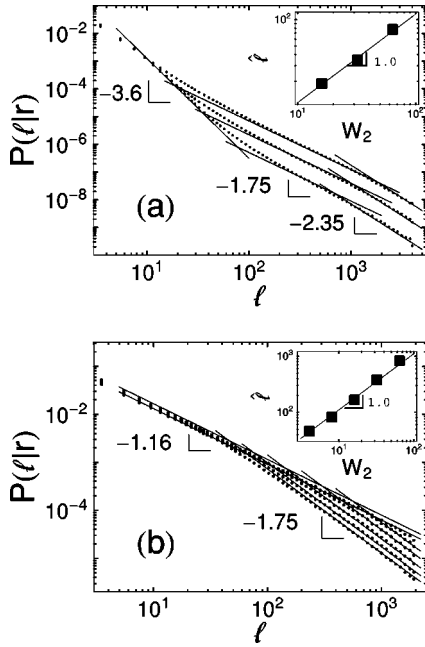


FIG. 8. $P(l|r)$ vs l for configurations of two lines of different lengths with $r=1$ and $W_1=128$. (a) $\theta=7^\circ$, W_2 =(from top to bottom) 16, 32, and 64. Three power-law regimes can be seen: the two-lines regime, the point-line regime, and the two-points regime. (b) $\theta=180^\circ$, W_2 =(from bottom to top) 4, 8, 16, 32, 64, and 128. Only the first two power-law regimes can be seen: the two-lines regime and the point-line regime (the two-points regime would require even larger values of l).

sliding the lines toward each other along the line of shortest Euclidean distance between the lines (without changing their orientations) until they touch; the lines are then coplanar and the angle between them determines the behavior of $P(l|r)$. Figure 10 contains plots for two configurations which illustrate this: (i) two coplanar lines with $r=1$, $\theta=90^\circ$, and $W=256$, and (ii) the same configuration with the second line translated out of the plane by distance 8. We see that while there is some difference in the plots for small l , the slope of the two-lines regime is the same for the two plots.

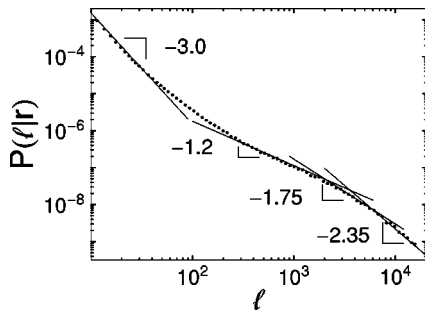


FIG. 9. $P(l|r)$ vs l for configurations of two lines of different lengths which “overlap” [see Fig. 1(c)] with $\theta=7^\circ$, $r=1$, $W_{1a}=32$, $W_{1b}=128$, and $W_2=256$. Four power-law regimes are present: the two-line ($\theta=7^\circ$) regime (slope -3.0), the two-line ($\theta=180^\circ-7^\circ$) regime (slope -1.2), the point-line regime (slope -1.75), and the two-points regime (slope -2.35).

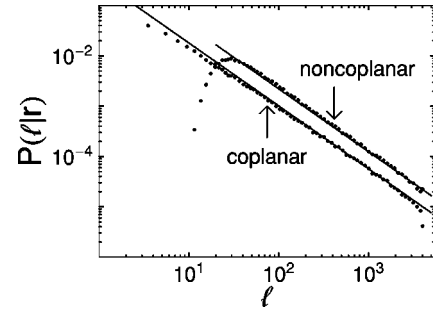


FIG. 10. $P(l|r)$ vs l for configurations of two lines of equal length. The coplanar configuration has $r=1$, $\theta=90^\circ$, and $W=256$ and the lines are coplanar. The noncoplanar configuration is obtained from the coplanar configuration by moving one of the lines a distance 8 perpendicular to the plane defined by the coplanar lines. One sees that for large l , the power-law regimes of the two plots have the same exponent.

C. Scaling of the crossover between power law regimes

We define the value of $l \cong \hat{l}$ at which $P(l|r)$ crosses over from one power-law regime to another power-law regime as the value of l where straight lines fit to the power-law regimes, between which the crossover takes place, cross. In Eq. (1) the values of l at which the lower and upper cutoffs occur scale independently as $r^{d_{\min}}$ and $L^{d_{\min}}$, respectively. By extension, we would expect that all characteristic values of the distribution, including crossovers between different power-law regimes, would also scale as $X^{d_{\min}}$ where X is the length in the system that controls the crossover. Thus, in analogy with the scaling of the most probable value of l, l^* ,

$$l^* = c r^{d_{\min}}, \quad (4)$$

we would, in fact, expect that the value of l, \hat{l} at which $P(l|r)$ crosses over from two-lines behavior to two-points behavior scales as

$$\hat{l} = c_1(\theta) r_{\max}^{d_{\min}}, \quad (5)$$

where

$$r_{\max} = r + 2W \sin(\theta/2) \quad (6)$$

is the maximum Euclidean distance between the two lines and $c_1(\theta)$ is a slowly varying function of θ . In order for a two-lines regime to exist, the two-lines regime cutoff \hat{l} must be greater than l^* , the maximum value of the distribution. That is,

$$c_1[r + 2W \sin(\theta/2)]^{d_{\min}} > c r^{d_{\min}}, \quad (7)$$

which implies

$$W > \frac{(c/c_1)^{1/d_{\min}} - r}{2 \sin(\theta/2)}. \quad (8)$$

In Figs. 4(a), 4(b), and 4(c), the insets contain plots of \hat{l} versus r_{\max} . For $\theta=3^\circ$, the scaling exponent is consistent with Eq. (5) but for $\theta=29^\circ$ and 180 the scaling exponent is 1.0 ± 0.1 .

Using the same reasoning that led to Eq. (5), we would expect the crossover from point line to two-points behavior to scale as

$$\hat{l} = c_2 W^{d_{\min}}, \quad (9)$$

because W is the length that controls this crossover; as seen in Fig. 7, the larger the value of W , the larger the value of l at which the crossover from point-line to two-points behavior occurs. However, as seen in the inset in Fig. 7, the crossover length scales with an exponent 1.0 ± 0.1 not d_{\min} .

Finally, we would expect that for different length lines, the crossover from two-lines behavior to two-point behavior would scale as

$$\hat{l} = c_3(\theta) W_2^{d_{\min}}, \quad (W_2 < W_1), \quad (10)$$

because W_2 is the length that controls this crossover; as seen in Fig. 8, the larger the value of W_2 , the larger the value of l at which the crossover occurs. Again, the insets in Fig. 8 indicate that the crossover scales with exponent 1.0 ± 0.1 .

We cannot explain why in some cases the crossover scales with d_{\min} and in others it scales with an exponent close to 1. It is, of course, possible that corrections to scaling are strong and that we are not seeing the true asymptotic behavior of the scaling of the crossover. These corrections to scaling might reflect the nondilute nature of the cluster close to the lines; a scaling exponent of 1 would be consistent with this nondilute regime. If this is the case, the question still remains as to why the corrections to scaling are strong in some configurations and not in others. This area is a subject for further study. Simulations for larger configurations than can feasibly be performed at present may help us understand the observed behavior of the crossover.

IV. PARALLEL WELLS

A. Simple configurations

As with nonparallel wells we first consider the simple configurations shown in Fig. 11(a) in which the parallel wells are of the same length. Figure 12(a) plots $P(l|r)$ versus l for $r=1$ and various W . The initial decay of the plots increases with increasing W because the longer the wells, the lower the probability for long shortest paths. Eventually, all plots cross over to a power-law regime with slope consistent with that for two points. To see if this initial decay is a lattice effect, Fig. 13 plots of the scaled distributions $r^{d_{\min}} P(l/r^{d_{\min}}|W)$ for various r and W where the aspect ratio,

$$R = \frac{W}{r}, \quad (11)$$

is fixed at $R=32$. Changing r and W but keeping R fixed results in scaling all lengths in the geometry by the same factor and the plots collapse as expected. Again, we note the

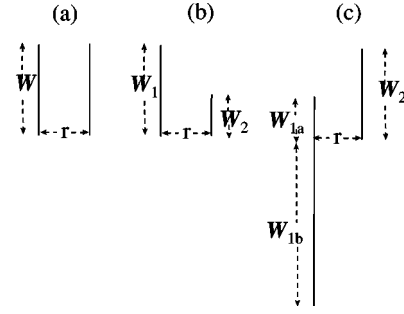


FIG. 11. Example configurations for parallel wells. (a) Simple configuration of wells of equal length. (b) Configuration of wells of unequal length ($W_1 > W_2$). (c) Configuration in which shortest line between the end of one well and the other well does not terminate at the end of the other well ($W_{1a} < W_2 < W_{1b}$).

initial strong decay of the distribution followed by a two-point power-law regime. The good collapse for small $x = l/r^{d_{\min}}$ indicates that the strong initial decay is not a lattice effect.

Because of the small values of l at which the crossover to the two-point regime occurs it is difficult to differentiate between a power law and (stretched) exponential decay. We will proceed as if the decay were either a power law with slope $\bar{g}(R)$ or equivalently an exponential with “effective slope” $\bar{g}(R)$.

One might argue as follows that the initial decay of $P(l|r)$ for parallel lines must be exponential: Since the two-lines regime of the probability distribution for a parallel well configuration must always decay faster than the two-lines regime of a configuration with small but nonzero θ and since we believe $g_l(\theta)$ goes to infinity as θ goes to zero, the decay for parallel lines must be exponential (i.e., faster than any power-law decay). This, however, need not be the case. In order for a two-lines regime to exist, Eq. (8) must hold. So as we decrease θ , we must increase W , increasing the aspect ratio R , to maintain a two-lines regime. But since the effective slope for parallel wells, $\bar{g}(R)$ increases with increasing R , the decay can be a power law and still always have a greater slope than the configuration with small but nonzero θ .

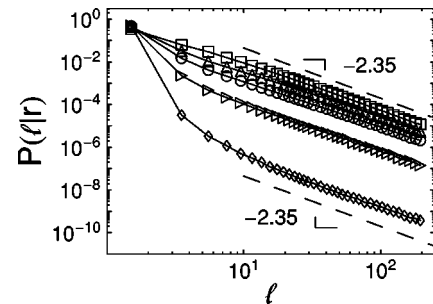


FIG. 12. $P(l|r)$ vs l for configurations of two parallel lines of equal length with $r=1$ and $W=($ from top to bottom) 0 (two points), 4, 8, 16, and 32. The slopes of the power-law regimes of the plots for all configurations are the same but the initial decay of the plots increases with increasing W .

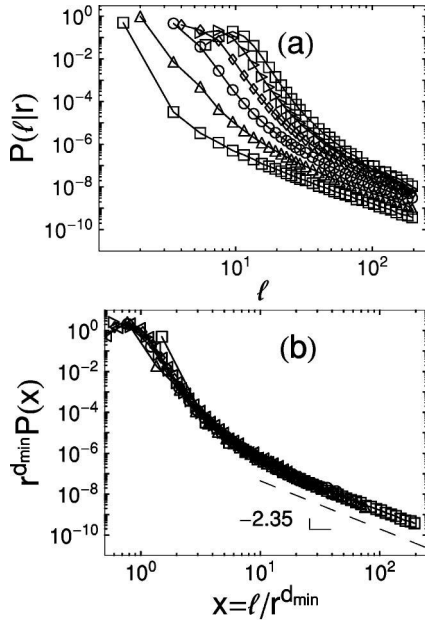


FIG. 13. $P(l|r)$ vs l for configurations of two parallel lines of equal length with $(W,r)=($ from top to bottom) $(32,1)$, $(64,2)$, $(96,3)$, $(128,4)$, $(160,5)$, and $(196,6)$, (b) plots of (a) scaled with the variable $x=l/r^{d_{\min}}$. The plots in (b) collapse nicely as would be expected since they all have the same aspect ratio, W/r . The good collapse for small x indicates that the small x behavior is not a lattice effect.

B. Complex configurations

The treatment of the more complex configurations shown in Figs. 11(b) and 11(c) follows that of nonparallel wells. $P(l|r)$ for configurations of the type in Fig. 11(b) would contain an initial two-line regime with slope $\bar{g}(R=W_2/r)$, a point-line regime, and finally a two-point regime. $P(l|r)$ for configurations of the type in Fig. 11(c), with $W_{1b} \ll W_2 \ll W_{1a}$ would contain an initial two-line regime with slope $\bar{g}(R=W_{1b}/r)$, a two-lines regime with slope $g_l(\theta=\pi)$, a point-line regime, and a two-point regime.

C. Quasi-Euclidean regime

When the length of the wells is very large and the distance between the wells is small the behavior of the most probable shortest path between the wells is close to a straight line. This can be seen in Fig. 14 in which we plot l^* , the most probable value of the shortest path, versus r for various lengths W . For long enough wells, there is a regime of r in which

$$l^* = r, \quad (12)$$

as one would expect in Euclidean space in which the shortest path is a straight line path of occupied bonds. As also seen in Fig. 14, for a given well length, as r increases, there is a value of r , r^* , at which the behavior crosses over to that of 3D percolation. We can develop a simple expression to estimate r^* as follows: The probability that all bonds in a straight line path between two wells separated by distance r

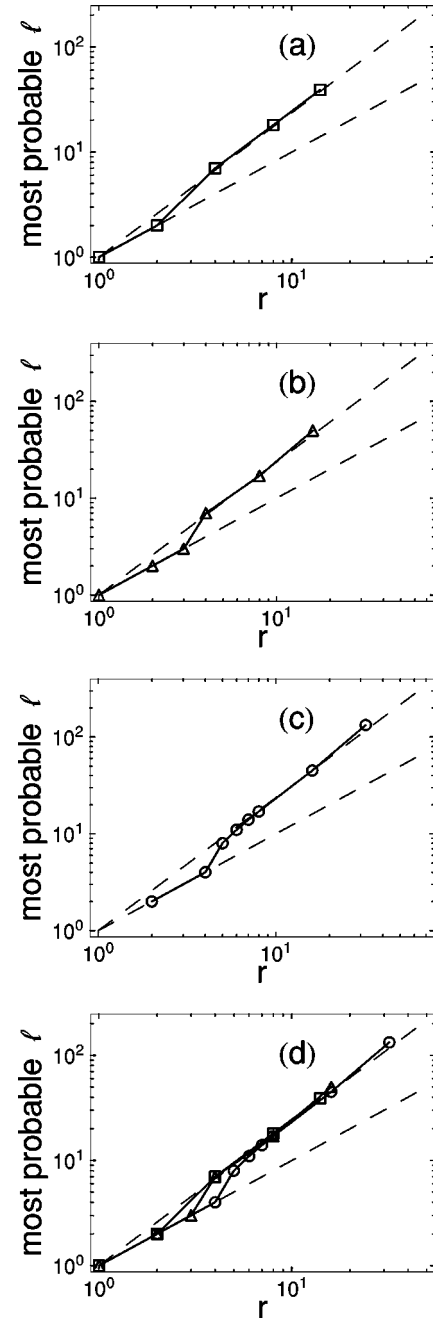


FIG. 14. Most probable l vs r for configurations of two parallel lines of equal length. (a) $W=16$, $r=1, 2, 4, 8$, and 14 . (b) $W=32$, $r=1, 2, 3, 4, 8$, and 16 . (c) $W=64$, $r=2, 4, 5, 6, 7, 8, 16$, and 32 . (d) Combined plot of (a), (b), and (c). The upper and lower dashed lines have slope d_{\min} (1.374) and 1.0, respectively. The larger the value of W , the larger the value of r at which scaling crosses over from Euclidean behavior to fractal behavior.

are occupied is p_c^r . The probability that one or more bonds in the straight line path is not occupied is thus $1-p_c^r$ and the probability that one or more bonds in the W possible straight line paths between the wells are not occupied is $(1-p_c^r)^W$. The probability that at least one straight line path has all bonds occupied is then

$$P(r,W) = 1 - (1-p_c^r)^W. \quad (13)$$

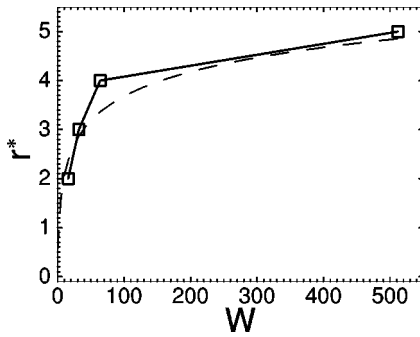


FIG. 15. Value of r at which behavior changes from linear to fractal, r^* , vs W . For $r < r^*(W)$, $l \sim r$ while for $r > r^*(W)$, $l \sim r^{d_{\min}}$. The dashed line is a prediction of Eq. (14).

The shortest path will exhibit linear behavior, $l^* = r$ when $P(r, W)$ is of the order unity. Setting $P(r^*, W) = a$ in Eq. (13), we find

$$r^* = \frac{\ln(1 - a^{1/W})}{\ln p_c}. \quad (14)$$

In Fig. 15 we plot the observed values of r^* and the values predicted by Eq. (14) with a value of $a = 0.55$ that gives the best fit to the observed values.

V. RELATIONSHIP BETWEEN PARALLEL WELLS AND “CLOSE TO PARALLEL” WELLS

For a given r , we expect that a configuration with a small but nonzero angle will have a power-law regime slope very close to the (effective) power-law regime slope of a configuration of parallel lines with the same W . This at first leads to a seeming paradox: If we increase or decrease W , but keep the angle of the nonparallel wells fixed, the slope of the two-lines regime of the nonparallel well configuration does not change as discussed in Sec. III A 1. However, if we consider this configuration as a parallel configuration, changing W changes the aspect ratio that changes the power-law regime slope as discussed in Sec. IV A. This seeming inconsistency is resolved as follows: On the one hand, for a two-lines regime to exist, W must be at least as large as the value given by Eq. (8). If W is too small, there will be no two-lines regime and both the parallel and small-angle configurations will look like the configuration for two points. On the other hand, if W is increased, keeping r and θ fixed, the greater is the deviation from parallel lines and there is no reason why the parallel and small-angle configurations should have the same slopes in their power-law regimes.

Thus, only for the very small range of W for which the power-law regime exists and for which the configuration with small but nonzero θ is “close to parallel” (i.e., the

difference between the values of r and r_{max} is small) should the slopes of the parallel configuration and the configuration with small but nonzero θ be equal. That is,

$$\bar{g}[W/r] \approx g_l(\theta), \quad (15)$$

where $\bar{g}(R)$ is defined in Sec. IV A.

VI. DISCUSSION AND SUMMARY

Motivated by the need to more realistically model the geometries found in oil recovery activities, we have determined the scaling form for the distribution of shortest paths between two lines in three-dimensional percolation systems. Using simple scaling arguments we explained the rich fractal behavior of the shortest path in these systems.

While it is doubtful that features other than the initial peak and the first power-law regime will be observed with measurements of actual oil fields, one can make the an important inference about the actual behavior of the distributions of shortest paths and breakthrough times: Because the slope of the power-law regime decreases with increasing angle between the wells, the uncertainty in the predicted shortest path or breakthrough times increases as the angle between the wells is increased. So, although certain operational considerations may favor configurations with large angles between the wells, a price is paid in the increased uncertainty in predictions of the most probable shortest path or breakthrough time.

A number of challenges, however, remain:

(i) Qualitatively, why does the power-law regime exponent $g_l(\theta)$ depend on angle? Why below some angle θ_c is $g_l(\theta)$ greater than the corresponding power-law exponent for the two-points configuration and smaller above θ_c ?

(ii) Can one develop an expression for $g_l(\theta)$? An exact expression for g_l for two points in two-dimensions was obtained by Ziff [5] using conformal invariance arguments of Cardy [14]. Possibly this approach could be extended to find g_l for point-line and two-line configurations, at least in two dimensions.

(iii) How is the fact that the crossover from one power-law regime to another does not scale with the exponent d_{\min} explained? Is this simply an artifact of corrections to scaling which would disappear if we could simulate much larger systems or is the scaling of the crossover actually anomalous in certain configurations?

ACKNOWLEDGMENTS

We thank Sergey Buldyrev, Nikolay Dokholyan, Youngki Lee, Eduardo Lopez, Peter King, and Luciano da Silva for helpful discussions and BP for financial support.

[1] N. V. Dokholyan, Y. Lee, S. V. Buldyrev, S. Havlin, P. R. King, and H. E. Stanley, *J. Stat. Phys.* **93**, 603 (1998); N. V. Dokholyan, S. V. Buldyrev, S. Havlin, P. R. King, Y. Lee, and H. E. Stanley, *Physica A* **266**, 53 (1999).

[2] Y. Lee, J. S. Andrade Jr., S. V. Buldyrev, N. Dokholyan, S. Havlin, P. R. King, G. Paul, and H. E. Stanley, *Phys. Rev. E* **60**, 3425 (1999).

[3] J. S. Andrade Jr., S. V. Buldyrev, N. Dokholyan, S. Havlin,

- P. R. King, Y. Lee, G. Paul, and H. E. Stanley, Phys. Rev. E **62**, 8270 (2000).
- [4] P. Grassberger, J. Phys. A **32**, 6233 (1999).
- [5] R. M. Ziff, J. Phys. A **32**, L457 (1999).
- [6] A. U. Neumann and S. Havlin, J. Stat. Phys. **52**, 203 (1988).
- [7] D. Stauffer and A. Aharony, *Introduction to Percolation Theory* (Taylor & Francis, Philadelphia, 1994).
- [8] *Fractals and Disordered Systems*, edited by A. Bunde and S. Havlin (Springer-Verlag, New York, 1996).
- [9] D. Ben-Avraham and S. Havlin, *Diffusion and Reactions in Fractals and Disordered Systems* (Cambridge University Press, Cambridge, England, 2000).
- [10] P. R. King, S. V. Buldyrev, N. V. Dokholyan, S. Havlin, Y. Lee, G. Paul, and H. E. Stanley, Physica A **274**, 60 (1999).
- [11] M. Sahimi, *Applications of Percolation Theory* (Taylor & Francis, London, 1994).
- [12] P. Grassberger, e-print cond-mat/0201313.
- [13] G. Paul, R. M. Ziff, and H. E. Stanley, Phys. Rev. E **64**, 026115 (2001).
- [14] J. Cardy, J. Phys. A **31**, L105 (1998).